Journal of Oceanography, Vol. 63, pp. 483 to 490, 2007

Short Contribution

Frequency-Wavenumber Spectra of Equatorial Waves Detected from Satellite Altimeter Data

YOSHINOBU WAKATA*

Research Institute for Applied Mechanics, Kyushu University, Kasuga-kohen, Kasuga-shi, Fukuoka 816-8580, Japan

(Received 11 May 2006; in revised form 18 December 2006; accepted 27 December 2006)

The sea surface height anomaly in the Pacific equatorial area was separated into equatorial modes using satellite altimeter data. The power-spectral density (PSD) was obtained for the east-west wavenumber and frequency for each separated mode. The PSD distribution was compared with the theoretical dispersion curve for the equatorial modes derived by Matsuno (1966). The first Rossby modes have a high-density distribution that is slightly lower than the theoretical dispersion curve, but the Kelvin mode and the higher Rossby modes have high-density distribution that almost matches each dispersion curve. Results of analyses of satellite observational data show that wave motion near the equator mainly shows characteristics of equatorial waves, especially for a intraseasonal time scale.

Keywords:
· Equatorial wave,
· mode separation,
· TOPEX/ POSEIDON,
· sea surface height,
· Pacific Ocean.

1. Introduction

The theoretical framework of the equatorial wave in meteorology was formulated by Matsuno (1966), who showed that wave motion in the equatorial region can be expressed by equatorial waves trapped in equatorial regions, which are inertia gravity waves, mixed Rossby gravity waves, Kelvin waves, and Rossby waves. Moore and Philander (1977) dealt with their respective applications to oceanography.

Until quite recently, *in situ* marine observation data were necessary to investigate equatorial waves in the ocean. A long time is needed to accumulate much data. Therefore, the annual variability related to wave motion was investigated mainly using climate data. Meyers (1979) described a wave motion that propagates westward by 0.58 m s^{-1} in the annual variation of the thermocline depth (14°C isothermal line) along the 6°N latitude line. Yu and McPhaden (1999) detected wave motion that propagates westward by 1.0 m s^{-1} along the 5°N latitude line and eastward by 0.5–0.7 m s^{-1} along the equator from climatological monthly data of mooring buoys of the Tropical Atmosphere Ocean (TAO) project, which NOAA/PMEL undertook. This propagation speed along the equator is far lower than the theoretical phase velocity of the Kelvin wave. Although that study did not present its results as those for the free Kelvin waves, their observational results are used herein for reference. The phase velocity of the Kelvin wave was estimated as 3.0 m s^{-1} near the date line (Eriksen *et al*., 1983) and as 2.3 m s^{-1} near the Galapagos Islands (Eriksen *et al*., 1983; Chelton *et al*., 1998) by solving an eigenvalue problem related to the stratification condition of their equatorial regions.

In recent years, satellite altimeter data have become increasingly useful for marine research in addition to *in situ* marine observation data. It has become possible to investigate oceanic wave motions continuously for long periods. Delcroix *et al*. (1991) estimated the phase velocity of the wave motion along the equator as 2.26 m s^{-1} eastward by calculating the lag correlation from Geosat satellite altimeter data for three months while the eastward wave propagation was clear. Moreover, Tapley *et al*. (1994) pursued the movement of a series of large sea surface height (SSH) anomalies related to wave propagation from TOPEX/POSEIDON satellite data, and estimated the speed of movement as 3 m s^{-1} eastward. These values resemble the theoretical phase velocity of the Kelvin wave calculated from the stratification condition. Satellite altimeter data are extremely useful for the study of wave propagation because they allow examination of the continuous behavior of the wave over time.

Many recent studies related to equatorial waves have used satellite altimeter data (Miller *et al*., 1988; Delcroix

* E-mail address: wakata@riam.kyushu-u.ac.jp

et al., 1991, 1994; Boulanger and Menkes, 1995; Boulanger and Fu, 1996; Wakata and Kitaya, 2002; Chelton *et al*., 2003). Miller *et al*. (1988), using Geosat satellite data, showed that Kelvin waves exist widely in a Pacific equatorial region. Delcroix *et al*. (1991) obtained the wave amplitude and phase velocity by finding the best fit of the Kelvin wave, of which the amplitude and phase velocity are unknown quantities, for the SSH anomaly. In this way, the phase velocity of the Kelvin wave was found to be 2.82 m s^{-1}. Moreover, the first mode of the Rossby wave was also calculated similarly, giving a phase velocity of 0.86 m s^{-1}. It is worth noting that temporal information was not used to estimate these phase velocities. Delcroix *et al*. (1994) performed equatorial mode expansion from SSH using the orthogonal property for the sum of zonal current and sea surface height anomalies, as applied by Wakata and Sarachik (1991) for the model output. Boulanger and Menkes (1995) and Boulanger and Fu (1996) also conducted mode expansion without using this orthogonal property; they used a singular value decomposition method. These studies investigated the role of equatorial waves on the occurrence or termination of El Niño. However, the propagation property of the wave in the wavenumber space was not discussed.

This paper is intended to elucidate the characteristics of wave propagation from the spectrum of the equatorial mode in the frequency-wavenumber space. We also describe the detection of the equatorial modes from satellite altimeter data. The equatorial waves are solutions of an eigenvalue problem; for that reason we call them equatorial modes, especially when they relate to mode-separation. We separate the sea surface height into equatorial modes using the best-fit method along the meridional direction. The power-spectrum density (PSD) is calculated for each equatorial mode using spectrum analysis to detect the equatorial modes. The waves must be equatorial free waves if high PSD concentrates near the theoretical dispersion curve derived by Matsuno (1966). By comparing the distribution of PSD with the theoretical dispersion curves, we can discover how well equatorial variability can behave under control of equatorial wave dynamics. The present study found that the concentration of high PSD is apparent mostly near the theoretical dispersion curve, especially for the intraseasonal time scale.

Section 2 explains the mode separation method. The PSD of ordinary time-space Fourier expansion at several latitudes is investigated in Section 3; the PSD of the equatorial modes is investigated in Section 4. Section 5 presents the conclusion and discussion.

2. Method of Mode Separation

Data used in the present study are sea surface height anomaly data (Delayed Time Map of Sea Level Anomaly: DT-MSLA), which are distributed by AVISO (2006), produced by composing data of multiple satellites such as TOPEX/POSEIDON, ERS, Jason-1, and Envisat. Data are recorded every 7 days, and are produced using data for 6 weeks. Therefore, phenomena with a time-scale of less than 14 days, which is the period corresponding to the Nyquist frequency, cannot be treated using these data. In addition, variability of less than 6 weeks might be weakened. The AVISO data are prepared for 1/4-degree intervals. The analyzed area is a rectangular area (20°S–20°N, 150°E–105°W). The analyzed period is about 13 years (October 1992–January 2006). The number of data for east-west is $N_x = 421$, that for north-south is $N_y = 161$, and time is $N_t = 693$: the total number is $N_x \times N_y \times N_t = 46{,}972{,}233$.

Data processing is performed for mode separation as follows: 1) The time mean is removed. 2) Zero padding is performed to increase the number of east-west data to $\tilde{N}_x = 1{,}024$. 3) Fourier expansion is performed east-west at each latitude. 4) Equatorial mode expansion is performed for each Fourier mode using best-fit method. 5) Time Fourier expansion is performed for the equatorial mode. In the above processing, processes 2) particularly have the following meaning. The minimum wavenumber can be made smaller in addition to permitting the use of FFT. Although it takes a smaller value mathematically, the east-west size of the Pacific Ocean provides a physical limitation. This wavenumber, which is relevant to the wavelength with the size of the Pacific Ocean, is 0.175 in nondimensional form. This limitation of the wavenumber demands attention. However, it is confirmed that the phase velocity can be estimated using two-dimensional FFT with zero padding for simulated data of sinusoidal waves with wavelengths that are twice that of the Pacific Ocean, migrating eastward in the Pacific Ocean. This limitation might be slightly extendable.

Because we use the best-fit method, space-Fourier expansion and time-Fourier expansion are not exchangeable. If time-Fourier expansion is executed first, the number of the best-fit modes is changed depending on the frequency. For that reason, calculation and interpretation become difficult if the operation is conducted in this order.

Analyses were performed in a nondimensional form with the representative length scale $L = (C/\beta)^{1/2} = 324$ km and time scale $T = (C\beta)^{-1/2} = 1.56$ days, which correspond to the phase velocity of the first baroclinic gravity mode $C = 2.4$ m s^{-1}. The β parameter is 2.29×10^{-11} $m^{-1}s^{-1}$. Consequently, the phase velocity of the Kelvin wave is also 2.4 m s^{-1} eastward.

Concrete calculations are explained below. Digital Fourier expansion is applied for SSH $h(x, y, t)$ after conducting the process up to 2) as

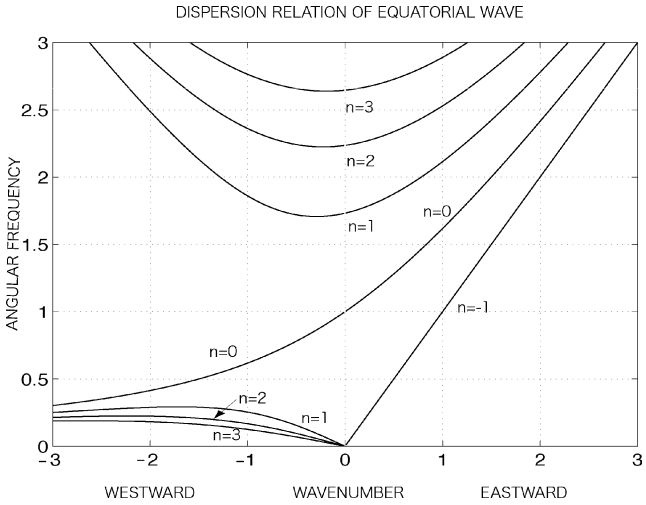

Fig. 1. Dispersion relation of the equatorial waves. Ordinate is a nondimensional angular frequency and the abscissa is a nondimensional wavenumber. Negative (positive) wavenumber indicates westward (eastward) propagation. Numbers n = 1, 2, ... in the low and left frequency-wavenumber space indicate the n-th Rossby mode, and n = 0 in the left space indicates the mixed Rossby gravity mode. Numbers n = 1, 2, ... in the upper space and n = 0 in the right space indicate the inertia gravity modes. The Kelvin mode is indicated by n = –1.

$$h(x,y,t)=\sum_{k_N=-\tilde{N}_x/2}^{\tilde{N}_x/2} h^k(y,t)\exp\left(2\pi i k_N x\Big/\left(\tilde{N}_x\Delta x\right)\right). \quad (1)$$

Wavenumber k corresponds to $2\pi k_N/(\tilde{N}_x\Delta x)$, where Δx is the nondimensional data interval in longitude. Because $h^{-k}(y, t)$ is the complex conjugate of Because $h^k(y, t)$, we will consider the positive wavenumber k only. The complex amplitude Because $h^k(y, t)$ of the mode for wavenumber k is expanded by equatorial modes $h_n{}^k(y)$ as

$$h^k(y,t)=\sum_{n=-1}^{N}\hat{h}_n^k(t)h_n^k(y). \quad (2)$$

The equatorial mode $h_n{}^k(y)$ is a meridional eigenmode of the equatorial wave with label n for a specified wavenumber k shown in Fig. 1. The form of $h_n{}^k(y)$ is mentioned later. The wave dispersion relation for the wave with the first baroclinic gravity mode in the vertical is drawn for positive frequency and positive-negative wavenumber in Fig. 1; this relation is symmetric with respect the origin in the frequency-wavenumber space. We must take up equatorial modes with negative wavenumber in Fig. 1, too, for mode separation because these modes exist in the 4th quadrant of the frequency-wavenumber space. Inertial gravity modes are not considered here because they have a high frequency that is larger than the Nyquist frequency of the data. Therefore, the Kelvin mode (n = –1), mixed Rossby gravity mode (n = 0), and Rossby modes ($n \geqq 1$) are considered for a specified wavenumber k. We take up four modes from first to fourth for the Rossby modes; thereby, the number N in Eq. (2) becomes 4. If one increases the mode further, the convergence of iteration worsens.

Amplitudes of equatorial modes with structure $h_n{}^k(y)e^{i(kx-\omega t)}$ for the SSH are expressed as follows:

The Kelvin mode is

$$h_{-1}^k(y)=A_{-1}\exp\left(-\frac{1}{2}y^2\right). \quad (3)$$

The mixed Rossby gravity mode is

$$h_0^k(y)=\frac{A_0}{\left(\omega^2-k^2\right)}\left(kyH_0+\omega yH_0\right)\exp\left(-\frac{1}{2}y^2\right); \quad (4)$$

and the n-th Rossby mode is

$$h_n^k(y)=\frac{A_n}{\left(\omega^2-k^2\right)}\left(kyH_n+\omega yH_n-2\omega nH_{n-1}\right)\exp\left(-\frac{1}{2}y^2\right) \quad (5)$$

where A_n is selected as the maximum value of $h_n{}^k(y)$ becomes 1. The angular frequency ω is calculated from the dispersion relation of the equatorial mode as

$$\omega^2-k^2-k/\omega=2n+1. \quad (6)$$

As noted above, SSH can be expressed by the composition of several Hermite functions $H_n(y)$.* The meridional cross sections of $h_n{}^k(y)$ are depicted in Fig. 2.

The amplitude $\hat{h}_n^k(t)$ of each mode in Eq. (2) is determined by the best-fit method as the following residual error becomes minimal:

*Hermite functions $H_n(y)$ are defined as

$$H_n(x)=(-1)^n e^{x^2}\frac{d^n}{dx^n}\left(e^{-x^2}\right) \text{ for } n\geq 1$$

and $H_n(x)$ = 1 for n = 0, and they have the following recursion formula: $H_{n+1}(x) = 2xH_n(x) - 2nH_{n-1}(x)$.

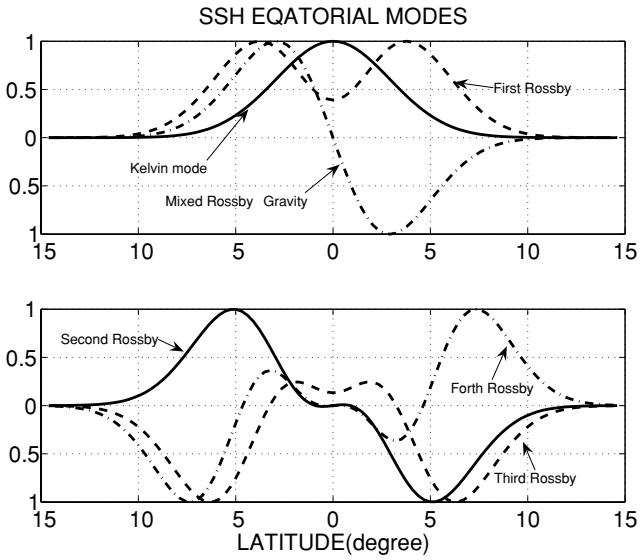

Fig. 2. Meridional section of SSH relevant to each equatorial mode with $k = 1$ (wavelength is 2,036 km). This is adjusted as the maximum becomes one. Abscissa is latitude in degree.

$$\Phi_k = \int_{y_s}^{y_n} \left\{ w(y) \left(h^k(y,t) - \sum_{n=-1}^{4} \hat{h}_n^k(t) h_n^k(y) \right)^2 \right\} dy, \quad (7)$$

where $w(y)$ is a weighting function and $w(y) = \exp(-(y/4)^2)$ is adopted. The accuracy of Hermite expansion becomes low for points that are distant from the origin, but wave activities still exist off the equatorial area. One has to contrive that the contribution decreases with the distant from the equator. The range of the weighting function is estimated from the approximate meridional scale of the adopted Rossby modes, as shown in Fig. 2. The results are not greatly affected by the choice of parameter near this value.

Next, the obtained $\hat{h}_n^k(t)$ is expanded into the Fourier series in time as

$$\hat{h}_n^k(t) = \sum_{\omega_N = -N_T/2}^{N_T/2} \hat{h}_n^{k,\omega} \exp\left(-2\pi i \omega_N t / (N_T \Delta T)\right). \quad (8)$$

The angular frequency ω corresponds to $2\pi\omega_N/(N_T\Delta T)$; ΔT is the data interval in time. Finally, the power spectrum density (PSD) is obtained as

$$\mathrm{PSD}_n(k,\omega) = \hat{h}_n^{k,\omega} \times \hat{h}_n^{k,\omega^*} / (N_x N_t). \quad (9)$$

The PSD is symmetric with respect to the origin in the frequency-wavenumber space; we produce the spectrum by transferring the PSD with positive wavenumber and negative frequency into that with negative wavenumber and positive frequency using this symmetry to compare the PSD with the wave dispersion in Fig. 1.

3. Frequency-Wavenumber Spectrum of SSH at Each Latitude

Ordinary two-dimensional spectrum analysis is conducted before proceeding to the equatorial mode separation. This calculation does not include the error related to the best-fit method for the equatorial mode separation. Therefore, it should be helpful in considering the validity of mode separation.

The time Fourier expansion is performed at several latitudes instead of process 4) of equatorial mode separation in Section 2. Figure 3 shows the $\log_{10}$(PSD) distribution. The nondimensional frequency 0.1 corresponds to 98 days, and the nondimensional wavenumber 1 to 2,039 km. Positive wavenumbers indicate eastward propagation; negative wavenumbers indicate westward propagation. The high PSD is distributed widely in wavenumbers for low frequencies that are common to all modes. A distribuion concentrated along a line is apparent for high frequencies.

In the case along the equator, PSDs around annual and semiannual periods (i.e. nondimensional frequency 0.027 and 0.054) extend widely in wavenumber space. Annual and semiannual variability might not behave as free modes, but as forced solutions. Regarding the high-frequency area, the high PSD is distributed along an inclined line. This inclination c is estimated by fitting a straight line passing through the origin (shown as a red line in Fig. 3) to the PSD distribution, as the following residual error becomes minimal:

$$\Psi = \sum_k \sum_\omega \left[\log_{10}(\mathrm{PSD}(k,\omega)) (\omega / c - k) \right]^2, \quad (10)$$

where PSDs satisfying the following conditions are used for this calculation. The adopted frequency domain is higher than 0.075. The nondimensional frequency of 0.075 corresponds to the period of 131 days; annual and semiannual variability are not included. The adopted wavenumber domain is $-3 < k < 0$ ($0 < k < 3$) for negative c (positive c). The threshold, over which PSDs are used for this calculation, is set as the magnitude of $\log_{10}(\mathrm{PSD}(k, \omega))$. This is one-half of the maximum $\log_{10}(\mathrm{PSD}(k, \omega))$ in the frequency-wavenumber domain described above.

The phase velocity can be estimated from this inclination. This phase velocity is 2.8 m s^{-1} eastward along the equator. Because the theoretical phase velocity of the Kelvin mode is 2.4 m s^{-1}, this result is likely to reflect the propagation of the Kelvin mode.

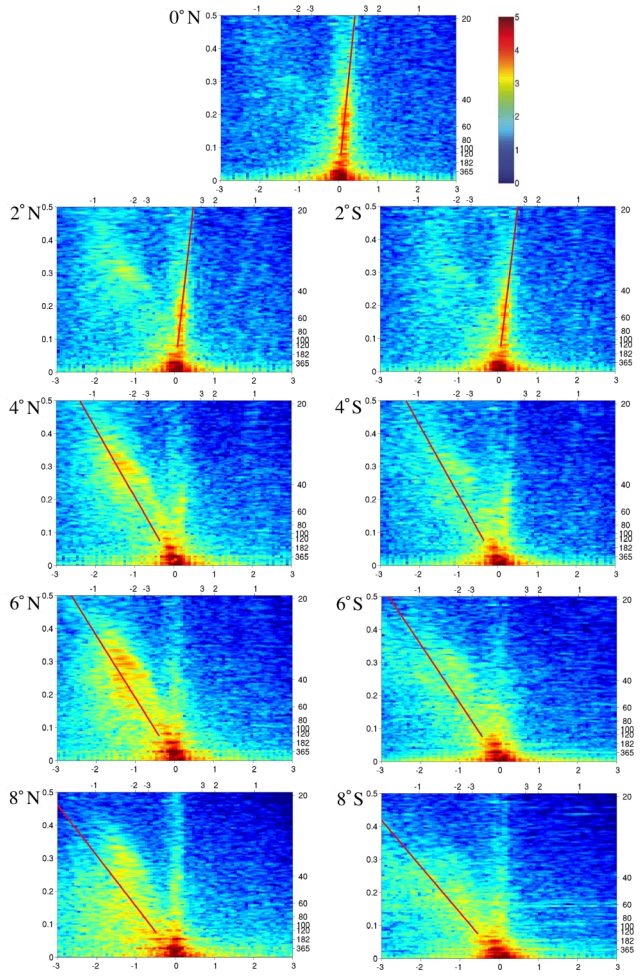

Fig. 3. Logarithm of PSD, that is $\log_{10}(\mathrm{PSD}(k, \omega))$, as estimated from the SSH at each latitude. Left ordinate is the nondimensionalized angular frequency. Right ordinate is the dimensional period (days). Bottom abscissa is the nondimensional east-west wavenumber. Top abscissa is the dimensional wavelength ($\times 10^3$ km). Best-fit lines are drawn in red.

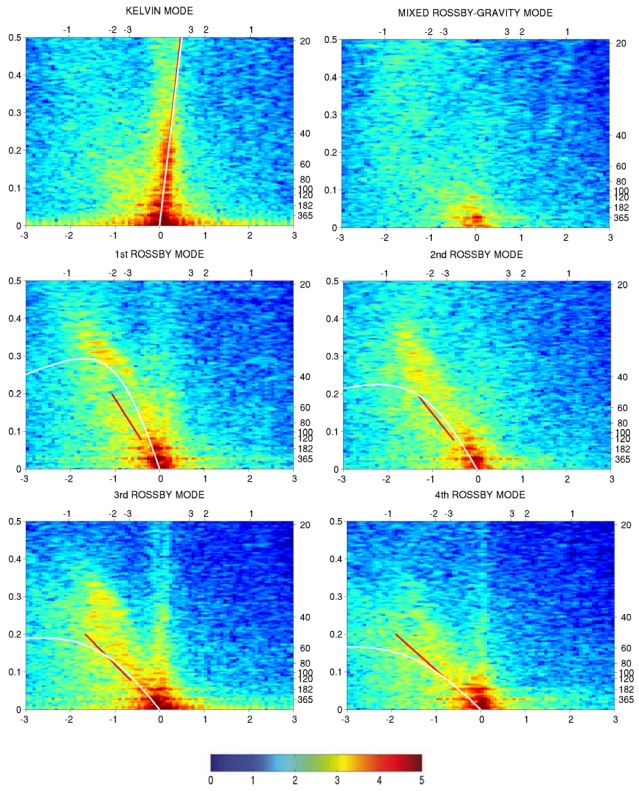

Fig. 4. Logarithm of PSD, that is $\log_{10}(\mathrm{PSD}(k, \omega))$, of each equatorial mode estimated from the SSH. Ordinate and abscissa are the same as Fig. 3. Theoretical dispersion curves in Fig. 1 are drawn in white and best-fit lines are drawn in red.

The left-inclined linear concentration of PSD is seen at latitudes from 2°N/S to 8°N/S in negative wavenumber space. The right-inclined ones are also seen up to 4°N/S from 0° in positive wavenumber space. The former signals come from the Rossby mode response; the latter arise from the Kelvin mode response. The spreading PSD left-right around annual (ω = 0.027) and semiannual (ω = 0.054) frequencies is especially apparent off the equator. This spreading might arise from the forced solution because of wind forcing. The estimation of phase velocity is also performed at several latitudes. The phase velocities are 2.51 m s^{-1} (2°N), 2.33 m s^{-1} (2°S); –0.50 m s^{-1} (4°N), –0.51 m s^{-1} (4°S); –0.46 m s^{-1} (6°N), –0.43 m s^{-1} (6°S); –0.37 m s^{-1} (8°N), and –0.34 m s^{-1} (8°S), respectively.

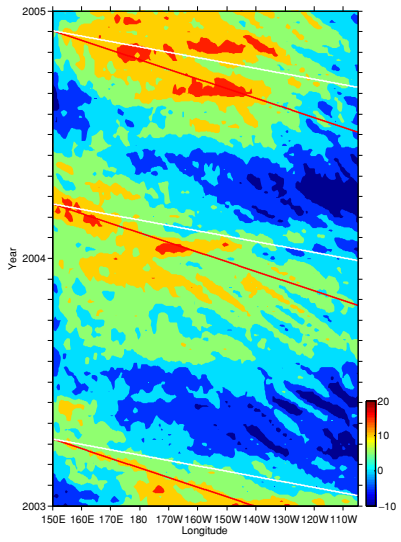

Fig. 5. Hovmöeller diagram (time vs. longitude) for the average of 4°N and 4°S SSHs. White line indicates the wave propagation, estimated from the theoretical phase velocity of –0.80 m s^{-1}. Red line is estimated from the present result of –0.45 m s^{-1}.

Zang *et al*. (2002) conducted a similar two-dimensional Fourier analysis for TOPEX/POSEIDON satellite SSH data. Their data were mapped onto a regular grid at intervals of 2 degrees longitude and 0.5 degrees latitude every 9.91 days using a Gauss filter. Their results showed a smaller signal in the high-frequency wavenumber domain than the present results for the 1/4-degree interval data. Consequently, their discussions mainly address annual and semiannual time-scale variability. They argue that the annual variability at 4°N is explained by the first meridional Rossby wave with second vertical mode. In the present results, the peak associated with annual variability at 4°N is located to the right of the theoretical dispersion curve of the first meridional Rossby wave with first vertical mode (Fig. 1). The dispersion curve with second vertical mode is located to the left of the first vertical mode. Therefore, the present results contradict their conjecture. However, limitations of Fourier analysis for the small wavenumber domain must be bore in mind.

We find some properties from this PSD. Its amplitude in the northern hemisphere is larger than that in the south, as indicated by Chelton *et al*. (2003). Meyers (1979) estimated the phase velocity of the off-equatorial nondispersive Rossby wave under the assumption of long waves as $c = -\beta g^* h_0 / f^2$ where g^* is a reduced gravity parameter and h_0 represents the depth of the thermocline. It is about –0.65 m s^{-1} at 6°N/S, which is greater than the present results; it is –0.30 m s^{-1} at 8°N/S, which is close to the present result. The wave is likely to behave as an off-equatorial Rossby wave in the area poleward from 8°N/S.

4. Frequency-Wavenumber Spectrum of Equatorial Modes

Ordinary two-dimensional spectrum analyses are somewhat affected by contamination caused by the mixing of some equatorial modes. For that reason, it would be difficult to discuss the behavior of the free equatorial mode. Here, the SSHs are separated into the equatorial modes using the best-fit method, as explained in Section 2. Figure 4 shows the distribution of PSDs of respective equatorial modes. The theoretical dispersion curve (Fig. 1) is also drawn with a white line in Fig. 4. The best-fit line is obtained similarly to the PSDs in the previous section; it is drawn as a red line.

For Kelvin modes, the white line's inclination indicates a phase velocity of 2.4 m s^{-1} of the theoretical Kelvin mode. The results show that the high PSD is distributed along the white line. The phase velocity of 2.5 m s^{-1} is obtained using the best-fit method (red line). This quantity is very close to that of 2.8 m s^{-1} estimated from the PSD along the equator in the previous section. The pattern of the PSD is also similar to that in Fig. 3. These results are quite consistent, indicating that the several modes aside from the Kelvin mode cancel each other out on the equator. The mode separation method is not likely to be influenced seriously by the error arising from the best-fit method.

The mixed Rossby mode has large frequency. The frequency at $k = 0$ corresponds to a period of 9.8 days. This is less than the Nyquist frequency of AVISO data. That with $k = -3$ is still a short period of 32 days. Consequently, this rapid variability must not be included in the original data. The PSD of the mixed Rossby gravity mode is indeed quite small, as shown in Fig. 4.

The high PSD of the first Rossby wave is distributed below the theoretical dispersion curve (white line), which indicates that the phase velocity is less than the theoretical value. The phase velocity is estimated as –0.45 m s^{-1} (i.e. westward) from the best-fit line (red line). For estimation of the best-fit line relevant to the Rossby modes, only PSD data satisfying both conditions $-3 < k < 0$ (i.e. longer than 678 km, but if the peak of the dispersion curve exists in this range, the wavenumber with the peak is used instead of the minimum wavenumber of –3) and $0.075 < \omega < 0.2$ (i.e. shorter than 131 days and longer than 49 days) are used to compare this result with the dispersion relation for the long wave. The phase velocity of the n-th Rossby mode is $-C/(2n + 1)$ (where C is the phase velocity of the Kelvin mode), which is based on the long wave assumption (i.e. small wavenumber k). This theoretical value of the first mode is –0.8 m s^{-1}. Therefore, the magnitude of the present phase velocity is 44% smaller than the theoretical one. The latitude where the amplitude of the first Rossby wave is large is about 4°N/S; the phase velocities near there are –0.50 m s^{-1} (4°N) and –0.51 m s^{-1} (4°S), as shown in Fig. 3. These values resemble the present result. This slow propagation of the first Rossby wave is acceptable in view of both results. However, it should be noted that two branches exist in the PSD distribution. The upper branch seems to be distributed along the theoretical dispersion curve (white line).

The phase velocity of the second Rossby mode estimated from PSD is –0.36 m s^{-1}, which is 25% less in magnitude than the theoretical value of –0.48 m/s. The third mode is –0.29 m s^{-1} and the theoretical value is –0.34 m/s. The speed is 15% less than theoretical value. The fourth mode is –0.25 m s^{-1} and is approximately equal to the theoretical value of –0.24 m s^{-1}, but the distribution of PSD is slightly divergent. The phase velocities of equatorial modes resemble the theoretical values, but the first Rossby mode is rather small. Equatorial wave disturbances, especially those with a intraseasonal time scale, are likely to behave as free equatorial modes.

5. Summary and Discussion

There are many studies related to the equatorial wave, which have used *in situ* data and satellite altimeter data, but only few such studies specifically address the dispersion relation. In the present study, the characteristics of

the equatorial mode were investigated from the perspective of the wave dispersion relation associated with equatorial wave theory. The SSHs composed from the satellite altimeter data (AVISO) are separated into equatorial modes using the best-fit method. The PSDs were obtained in the frequency and wavenumber space using spectral analyses. The wave dispersion relation was then discussed from this result.

The PSDs related to the Kelvin mode are distributed along the theoretical dispersion line, especially for the high frequency, such as intraseasonal time scale. The mixed Rossby gravity mode is small because of the large frequency, which is larger than the Nyquist frequency of the original data. The phase velocity of the first Rossby mode is 44% smaller than the theoretical value, but those of higher Rossby modes are close to the theoretical value. The results described here, from the frequency-wavenumber power spectrum of each mode, showed that equatorial wave disturbances, especially with the intraseasonal time scale, behave mainly under the control of classical equatorial wave dynamics.

Numerous studies have addressed annual variability using *in situ* marine observations (Meyers, 1979; Yu and McPhaden, 1999). The propagation speed of the wave differs from the theoretical value. In the present study it was difficult to find the clear wavenumber dependence in PSD for low frequency, because PSD is widely spread over wavenumbers. If we use data with time-scale longer than 131 days, i.e. $\omega < 0.075$ for calculation of the best-fit line, the estimated phase velocity of the Kelvin mode becomes the smaller value of 0.33 m s^{-1}. This fact might be related to the low phase velocity estimated from *in situ* annual data. External forcing related to the annual and semiannual variability has a coherent structure in space and time. Hence, the equatorial waves excited by these forcings become forced solutions rather than free modes.

The small phase velocity of the first Rossby modes is confirmed directly from the Hovmöeller diagram of SSH data (AVISO). Figure 5 shows the Hovmöeller diagram for the average of 4°N and 4°S SSHs, where the first Rossby mode has peaks (Fig. 2). The characteristic line (white), estimated from the theoretical phase velocity of –0.80 m s^{-1}, indicates the apparent overestimation of phase velocity for the westward migration of some distinguishable SSH peaks in the western part. Meanwhile, the red line, estimated from the present research of –0.45 m s^{-1}, gives a better estimation. It is certain that the phase velocity of the first Rossby mode is smaller than theoretical estimation. It is noted that the eastward propagating signal associated with the Kelvin modes is also seen. Furthermore, more or less regular wavelike signals are seen propagating westward in the eastern part, which result from the tropical instability waves with short period and wavelength. This phase velocity is further small.

The reason for reducing phase velocity of the first Rossby mode is that the Rossby mode might be affected by the second vertical modes or the background flow associated with the equatorial under-current. An eastward flowing under-current exists in the narrow area of 2°S–2°N under the thermocline at up to 250 m depth, having its core at 100 m. Philander (1979) calculated the phase velocity in the two-layer fluid considering the effect of the under-current. These results show that the phase velocity was reduced (figure 6 in Philander (1979)). This might explain the good agreement of the higher Rossby modes with the theoretical value that these modes have larger amplitude poleward than the under-current. This should be confirmed from the eigenvalue problem.

Some features are also found in PSD in addition to aligned distribution along the theoretical dispersion line. On the intraseasonal time-scale, some peaks in PSD are apparent for the ordinary spectrum at the equator (Fig. 3) and for the Kelvin mode (Fig. 4). Peaks exist around 120-day and 70-day periods, as Cravatte *et al*. (2003) described. They noted that the 120-day signal comes from the second vertical modes. The high spot of PSD is found around the 30 day period and 1500 km in Fig. 3 (2°N–6°N). An instability wave is known to exist in equatorial areas (Legeckis, 1977), which is also seen in the Hovmöeller diagram of SSH (Fig. 5). This wave extends in the area 2°N–6°N of the eastern Pacific; its period is about 30 days and the wavelength is about 1500 km. The nondimensionalized wavenumber is 1.3 and the frequency is 0.33. The spot relates to this instability wave. Estimation of the phase velocity of the westward propagating signal owing to the ordinary two-dimensional spectrum analysis might be influenced by this instability wave. Its influence on mode separation is likely to be limited because high-frequency data are not used for estimating the phase velocity for mode separation.

Some points of this study are particularly noteworthy. The phase velocity was calculated from the best-fit line. The estimation of the best-fit line depends somewhat on the cutoff in the frequency-wavenumber space and the PSD threshold. Selection of the cutoff frequency presents some ambiguity, but we adopted it to avoid annual and semiannual signals that might yield a forced solution. It should be recalled that the present estimated phase velocity comes from intraseasonal time-scale data.

The thermocline depth is deep in the western and shallow in the eastern Pacific. This spatial difference might also affect the present research. We adopted the phase velocity of the first gravity mode as $C = 2.4$ m s^{-1} in the present research, which is proportional to the square root of thermocline depth. This value is a little large in the western Pacific Ocean, as discussed in the first section. To check the sensitivity of this value, we recalculate the results with adopting $C = 2.7$ m s^{-1} instead of 2.4 m s^{-1}. The estimated phase velocity of Kelvin mode in-

creases to 2.8 m s^{-1} but those of Rossby modes are almost unchanged and the deformation of PSDs is quite small. Hence, the sensitivity to the selection of C is not great. However, one must be cautious about the following point. The phase velocity of equatorial mode was estimated in the present study, but this is not the best method for this purpose. The phase velocity must change according to location owing to the local variability of the wave medium. To obtain the accurate phase velocity, it may be better to estimate the phase velocity locally using a lag correlation method for the time-filtered data. Since the main purpose of the present study is to compare the PSDs and the theoretical wave dispersion, the present analysis used all east-west data. This problem must be reflected in the result. This might divert the PSDs somewhat from the theoretical dispersion curve.

Comparing the PSDs of equatorial mode (Fig. 4) with that of the ordinary two-dimensional spectrum (Fig. 3), PSDs of each mode generally resemble that of an ordinary two-dimensional spectrum at a latitude which corresponds to the location of each mode peak. However, the mixed Rossby gravity mode has small amplitude, and PSDs of higher Rossby modes are slightly more inclined to the left than an ordinary spectrum, which gives a good phase velocity. These points suggest that the mode contamination included in the ordinary spectrum is appreciably reduced and mode separation seems to work well.

There are differences of PSDs of the ordinary spectrum in northern and southern hemispheres shown in Fig. 3: the northern amplitude is larger than that in the southern hemisphere. Chelton *et al*. (2003) pointed out that the Rossby mode has an asymmetric meridional structure against the equator when one considers background flow. The structure of the mode treated here is only symmetric or antisymmetric, and the present investigation specifically examines how classical equatorial wave theory based on no background flow is applicable to the equatorial ocean. Future research will include asymmetric modes.

Acknowledgements

The author gratefully acknowledges the use of data (DT-MSLA: Delayed Time Map of Sea Level Anomaly) distributed by AVISO, and wishes to express his thanks to two reviewers: their comments were very helpful in improving this article.

References

AVISO (2006): SSALTO/DUACS User Handbook: (M)SLA and (M)ADT near-teal time and delayed time products. Publ., CLS-DOS-NT-06.034, France.

Boulanger, J.-P. and L.-L. Fu (1996): Evidence of boundary reflection of Kelvin and first-mode Rossby waves from TOPEX/POSEIDON sea level data. *J. Geophys. Res.*, **101**, 16361–16371.

Boulanger, J.-P. and C. Menkes (1995): Propagation and reflection of long equatorial wave in the Pacific ocean during the 1992–1993 El Niño. *J. Geophys. Res.*, **100**, 25041–25095.

Chelton, D. B., R. A. d. Szoeke, M. G. Schlax, K. E. Naggar and N. Siwertz (1998): Geographical variability of the first baroclinic Rossby radius of deformation. *J. Phys. Oceanogr.*, **28**, 433–460.

Chelton, D. B., M. G. Schlax, J. M. Lyman and G. C. Johnson (2003): Equatorially trapped Rossby waves in the presence of meridionally sheared baroclinic flow in the Pacific Ocean. *Prog. Oceanogr.*, **56**, 323–380.

Cravatte, S., J. Picaut and G. Eldin (2003): Second and first baroclinic Kelvin modes in the equatorial Pacific at intraseasonal timescales. *J. Geophys. Res.*, **108**, 3266, doi:10.1029/2002JC001511.

Delcroix, T., J. Picaut and G. Eldin (1991): Equatorial Kelvin and Rossby wave evidenced in the Pacific ocean through Geosat Sea level and surface current anomalies. *J. Geophys. Res.*, **96**, 3249–3262.

Delcroix, T., J.-P. Boulanger, F. Masia and C. Menkes (1994): Geosat-derived sea level and surface current anomalies in the equatorial Pacific during the 1986–1989 El Niño and La Niña. *J. Geophys. Res.*, **99**, 25093–25107.

Eriksen, C. C., M. B. Blumenthal, S. P. Hayes and P. Ripa (1983): Wind-generated equatorial Kelvin wave observed across the Pacific Ocean. *J. Phys. Oceanogr.*, **13**, 1622–1640.

Legeckis, R. (1977): Long waves in the eastern equatorial Pacific; a view from a geostationary satellite. *Science*, **197**, 1177–1181.

Matsuno, T. (1966): Quasi-geostrophic motions in equatorial areas. *J. Meteor. Soc. Japan*, **44**, 25–43.

Meyers, G. (1979): Annual variation in the slope of the 14°C isotherm along the equator in the Pacific ocean. *J. Phys. Oceanogr.*, **9**, 885–891.

Miller, L., R. Cheney and B. Douglas (1988): GEOSAT altimeter observations of Kelvin waves and the 1986–1987 El Niño. *Science*, **239**, 52–54.

Moore, D. W. and S. G. H. Philander (1977): Modeling of tropical oceanic circulation. p. 319–361. Vol. 6, *The Sea*, Wiley (Interscience).

Philander, S. G. H. (1979): Equatorial waves in the presence of the equatorial undercurrent. *J. Phys. Oceanogr.*, **9**, 254–262.

Tapley, B. D., D. P. Chamber, C. K. Shum, R. J. Eanes, J. C. Ries and R. H. Stewart (1994): Accuracy assessment of the large-scale dynamic ocean topography from TOPEX/POSEIDON altimetry. *J. Geophys. Res.*, **99**, 24605–24617.

Wakata, Y. and S. Kitaya (2002): Annual variability of sea surface height and upper layer thickness in the Pacific Ocean. *J. Oceanogr.*, **58**, 439–450.

Wakata, Y. and E. S. Sarachik (1991): On the role of equatorial ocean models in the ENSO cycle. *J. Phys. Oceanogr.*, **21**, 434–443.

Yu, X. and M. J. McPhaden (1999): Seasonal variability in the equatorial Pacific. *J. Phys. Oceanogr.*, **29**, 925–948.

Zang, X., L.-L. Fu and C. Wunsch (2002): Observed reflectivity of the western boundary of the equatorial Pacific Ocean. *J. Geophys. Res.*, **107**, C10, 3150, doi:10.1029/2000JC000719.